Phase transitions in spin-orbital models with spin-space anisotropies for iron pnictides: Monte Carlo simulations

Ryan Applegate, Rajiv R. P. Singh, Cheng-Chien Chen, and Thomas P. Devereaux

Phys. Rev. B **85**, 054411 — Published 9 February 2012

DOI: 10.1103/PhysRevB.85.054411

Phase transitions in spin-orbital models with spin-space anisotropies for iron-pnictides: A study through Monte Carlo simulations

Ryan Applegate and Rajiv R. P. Singh
University of California Davis, CA 95616, USA

Cheng-Chien Chen and Thomas P. Devereaux
Stanford Institute for Materials and Energy Science,
SLAC National Accelerator Laboratory, Menlo Park, California 94025, USA and
Geballe Laboratory for Advanced Materials, Stanford University, Stanford, California 94305, USA
(Dated: January 19, 2012)

The common phase diagrams of superconducting iron pnictides show interesting material specificities in the structural and magnetic phase transitions. In some cases the two transitions are separate and second order, while in others they appear to happen concomitantly as a single first order transition. We explore these differences using Monte Carlo simulations of a two-dimensional Hamiltonian with coupled Heisenberg-spin and Ising-orbital degrees of freedom. In this spin-orbital model, the finite-temperature orbital-ordering transition results in a tetragonal-to-orthorhombic symmetry reduction and is associated with the structural transition in the iron-pnictide materials. With a zero or very small spin space anisotropy, the magnetic transition separates from the orbital one in temperature, and the orbital transition is found to be in the Ising universality class. With increasing anisotropy, the two transitions rapidly merge together and tend to become weakly first order. We also study the case of a single-ion anisotropy and propose that the preferred spin-orientation along the antiferromagnetic direction in these materials is driven by orbital order.

PACS numbers: 74.70.Xa,75.25.Dk,75.40.Cx,75.40.Mg

I. INTRODUCTION

Several parent phases of the superconducting iron-pnictide materials show an interesting interplay of structural, magnetic and orbital degrees of freedom.[1–3] These quasi two-dimensional (2D) materials share a similar phase diagram, where a tetragonal paramagnetic phase at high temperatures transitions into an orthorhombic, antiferromagnetic phase at low temperatures.[4–9] The square-lattice of iron atoms develop magnetic order at wavevector $(\pi, 0)$, which corresponds to antiferromagnetic (AFM) alignment of spins along one of the nearest-neighbor direction (x) and ferromagnetic (FM) alignment along the other (y).[10–19] The orientation of the ordered spin moments is tied to antiferromagnetism and points along the AFM direction.[13–19]

While lattice distortions are typically quite small in iron pnictides, the observed spin-wave spectra from neutron scattering suggest a robust, possibly sign changing anisotropy in the exchange constants along the x and y directions.[20–22] Various transport, optical, and spectroscopic measurements also show substantial emergent anisotropies in the 2D xy plane.[23–32] In particular, an orbital polarization associated with the occupation of d_{xz} and d_{yz} orbitals has been observed.[33–36] These anisotropies in some cases can persist up to high temperatures and have been identified with long and sometimes short range Ising-nematic order.[37,38]

Despite the above similarities, there are also substantial material-specific differences. The parent compounds of the 1111 family (RFeAsO, with R a rare earth element) of iron pnictides undergo two separate second order phase transitions, where the structural transition is followed by a magnetic transition at a lower temperature.[6] On the other hand, in the 122 family (AFe_2As_2, with A an alkaline earth element) the two transitions appear to occur at the same temperature.[7–9]

More recent measurements revealed that in the undoped $BaFe_2As_2$, the structural and magnetic transitions are slightly separated by less than one Kelvin.[39–41] In that case, the structural transition starts as second order, and at a slightly lower temperature there is a first order jump in the lattice distortion with a concomitant first order magnetic transition. This feature is not generic to all the 122 family of iron pnictides. In particular, there is strong evidence showing a largely first order phase transition in $CaFe_2As_2$ and $SrFe_2As_2$, where the structural and magnetic phase transitions coincide.[42–44]

There have been many proposals for the mechanism driving these transitions. These include, (i) emergent Ising nematic orders in frustrated spin systems,[37,38,45–53] (ii) orbital order[54–63] (iii) coupling to lattice degrees of freedom,[64,65] and (iv) symmetry breaking associated with fermi-surface effects in an itinerant system.[65–70] On symmetry grounds one cannot distinguish between different pictures, since the different degrees of freedom lead to same broken symmetries and they are all present to some extent and coupled to each other. Thus, detailed quantitative studies are important to establish the role played by different mechanisms.

In this paper, we wish to study the scenario where orbital order is the primary driving mechanism for the finite temperature transitions. We investigate the properties of a spin-orbital model, where the spin and orbital

degrees of freedom are coupled by a Kugel-Khomskii like mechanism.[71] In the model, the local orbital occupation modulates the spin exchange constants. Once the orbitals are ordered, collinear antiferromagnetism can develop and anisotropic exchange constants in the x and y directions $J_{1x} \neq J_{1y}$ result. However, we note that a model containing only effective Heisenberg spin interactions ($\sum_{ij} J_{ij}\vec{S}_i \cdot \vec{S}_j$) is still *isotropic in spin space*, since the energy of the system does not depend on the direction of magnetization with respect to the crystal axes.

A simple mean-field treatment of our spin-orbital model suggests that the spin and orbital orderings occur simultaneously as a single phase transition, which can be first or second order depending on the exchange couplings. However, such a treatment neglects long-wavelength fluctuations which can drive the spin-ordering temperature to zero. To study the effects of fluctuations, we employ large scale Monte Carlo simulations by treating the spin and orbital variables classically, which should be sufficient for finite-temperature phase transitions. The Monte Carlo results indicate that if spin rotational invariance is preserved, at finite temperatures there is only one orbital ordering transition which belongs to the 2D Ising universality class. In this case, long-range spin order only occurs at $T = 0$, in accord with the Mermin-Wagner theorem. However, a small spin space anisotropy (5%) will bring the magnetic transition temperature up to the orbital one. With increasing anisotropy the coupled spin-orbital transition tends to become first order. These results are reminiscent of the observed behaviors of different families of iron pnictides.

Our study neglects three-dimensional (3D) couplings, studied for example in Refs. 38, 51 and 53. 3D couplings have a similar effect as spin space anisotropies in that they both can result in a finite-temperature magnetic transition. However, in general they will lead to different universality classes for the transitions. While 3D couplings could be more important in some materials (for example within the 122 family), spin space anisotropy may be more important in others. In some materials the magnetization has been reported to obey 2D Ising universality behavior.[76] Even if the ultimate transition is weakly first order in these materials, the reported fluctuations appear more 2D. This provides a motivation for our choice of anisotropy over 3D couplings.

Studying spin space anisotropy also allows us to address the orientation of the ordered moments. In a quasi-two dimensional material, one would expect the uniaxial anisotropy to point out of the plane and the spins should be equally likely to point along any direction in the plane. However, this can change with orbital polarization. In transition metal compounds, ligand crystal-field splitting can lift the degeneracy of the transition metal $3d$ orbitals. In this case, the orbital moments are usually quenched and there may be no preferred spin directions. However, relativistic spin-orbit coupling can induce a non-zero orbital angular momentum, which accompanied by an orbital polarization (such as a preferential occupation of d_{xz} over d_{yz} orbitals) can lead to a single-ion anisotropy term and an anisotropic g-factor in the xy plane. In this case, excess population of d_{xz} orbitals can favor spins pointing along the x-axis, while excess population of d_{yz} orbitals will favor spins pointing along the y direction. We propose that in iron pnictides the single-ion anisotropy term in the xy plane is related to orbital order and since it is also tied to AFM it leads to spins pointing along the AFM direction.

The outline of the paper is as follows. In section II we introduce our model and develop a simple mean field theory. In section III the Monte Carlo results are discussed. In section IV we discuss the implication of our study for the iron pnictide materials and in section V we summarize our work. Details of the Monte Carlo method are presented in the appendix.

II. II. SPIN-ORBITAL MODEL

The spin-orbital model is given by the Hamiltonian,

$$\begin{aligned} H = & \sum_i (J_1 n_i n_{i+\hat{x}} - J_F)\vec{S}_i \cdot \vec{S}_{i+\hat{x}} \\ & + \sum_i (J_1(1-n_i)(1-n_{i+\hat{y}}) - J_F)\vec{S}_i \cdot \vec{S}_{i+\hat{y}} \\ & + \sum_{<<i,j>>} J_2 \vec{S}_i \cdot \vec{S}_j \ . \end{aligned} \tag{1}$$

Here $\vec{S}_i$ are classical Heisenberg spins on a square-lattice, n_i are classical Ising variables that take values 0 or 1, and $<< i, j >>$ signifies summing on next nearest neighbor pairs of the square-lattice. In a classical system the spin magnitude S is not important in determining the phase transitions, and for our discussion we set $S = 1$. Physically, the variables n_i represent the preferential occupation of d_{xz} ($n_i = 1$) or d_{yz} ($n_i = 0$) orbitals. The model has tetragonal symmetry. However, $n_i = 1$ (occupation of d_{xz} orbitals) favors AFM order along the x-axis, whereas $n_i = 0$ (occupation of d_{yz} orbitals) favors AFM order along the y-axis. We have added an orbital independent FM nearest neighbor interaction J_F and used $J_2 = 0.4J_1$ and $J_F = 1/6J_1$. This set of parameters corresponds to the neutron scattering observation that the spin-wave spectra is better fit with an AFM exchange along one direction and a weak FM exchange along the other.[73] The latter could arise from double exchange[57] or from the orbital geometries.[55] But, its sign or magnitude is not crucial for the phase transitions we report here. Spin-space anisotropies will be introduced later when we discuss the Monte Carlo simulations.

The ground state of this model breaks tetragonal symmetry. It has a ferro-orbital order, all $n_i = 1$ or $n_i = 0$, corresponding to nearest neighbor exchanges which are AFM along one axis and FM along the other. The ground state has $(\pi, 0)$ spin order when $n_i = 1$ and $(0, \pi)$ spin order when $n_i = 0$.

We note here that in iron pnictides, the low temperature orbital polarization is found to be incomplete, where the occupation number is not strictly one or zero.[33–36] A partial orbital polarization can result from the itinerant electron degrees of freedom, or from quantum fluctuations in the orbital variables. The role of orbital order in driving the structural and magnetic transitions of iron pnictides indeed has been discussed based on an itinerant electron perspective using multi-orbital Hubbard Hamiltonians.[59–62] Our approach of studying a Kugel-Khomskii type spin-orbital model can be viewed as the strong coupling limit of such Hamiltonians. While we leave out the charge degrees of freedom which are important in describing for example transport properties, our model should still capture the key physics of magnetism and finite temperature phase transitions.

Below we first develop a mean-field theory for the phase transitions of the spin-orbital model under consideration. We set $n_i = (1+\sigma_i)/2$ and assume a mean-field Hamiltonian of the form

$$\mathcal{H}_{MF} = -\sum_{i1} B_1^{i1} S_{i1} - \sum_{i2} B_2^{i2} S_{i2} - h\sum_i \sigma_i \quad (2)$$

where the first sum runs over sublattice one, the second over sublattice two, and the third over all the spins in the lattice. B_1 and B_2 are the staggered fields on the two sublattices and h is a field that couples to orbital order. Focusing on the $(\pi, 0)$ order, we let $m = \langle S_i \rangle$ and $n = \langle \sigma_i \rangle > 0$. We find for $i = 1, 2$

$$B_i = 2m(J_1 n + 2J_2), \qquad h = J_1 m^2, \quad (3)$$

leading to the mean-field equations,

$$m = L(2\beta m(J_1 n + 2J_2)), \quad (4)$$

and

$$n = \tanh(\beta J_1 m^2). \quad (5)$$

Here, $L(x)$ is the Langevin function $\coth x - 1/x$. These equations lead to a simultaneous transition and an orbital ordered AFM phase. It is a second order phase transition, with a transition temperature of $4J_2/3$, provided $J_2 >$ constant J_1. The transition becomes first order when J_1 exceeds J_2 (the case of interest in the pnictides).

While mean-field theory can not be quantitatively valid because of the divergent infrared fluctuations in the spin variable, which push the spin ordering transition temperature to zero, we will see that the mean-field results correctly capture the following physics:

1. Non-zero magnetic order produces an ordering field for the orbital degrees of freedom. Hence, whenever there is magnetic order present, orbitals symmetry will also be broken. Thus, orbital transition can not happen below the magnetic ordering transition.

2. Without some order of the magnetic degrees of freedom, the orbitals do not interact. Actually, orbital couplings depend on short-range magnetic order not long-range magnetic order. This is not allowed for in the mean-field theory but will become clear from our later discussion of the Monte Carlo simulations. Thus, the two transitions are always going to be close in temperature, unless the magnetic transition is pushed significantly below the mean-field transition temperature due to additional fluctuations.

3. The orbital ordering temperature is not significantly depressed by the fluctuations of the spins and our mean field theory provides a fairly good prediction of the transition temperature.

4. We will see in the Monte Carlo simulations that the main role of the long-wavelength spin fluctuations is to decouple the spin and orbital transitions. The spin transition temperature is pushed to zero in the absence of spin space anisotropy. In this case, the orbital transition becomes Ising like and second order.

5. With significant anisotropy, both the spin and orbital transition temperatures rapidly approach the mean-field values, and the transition has a tendency to become first order for $J_1 > J_2$.

III. III. RESULTS OF MONTE CARLO SIMULATIONS

In this section, we present the results of Monte Carlo simulations with and without spin-space anisotropies. The details of the Monte Carlo methods as well as the quantities measured and the expected scaling behavior are discussed in the appendix.

A. Isotropic Heisenberg Spins

First, we consider the case of isotropic Heisenberg spins. The squares of spin and orbital order parameters obtained from the simulation are shown in Fig. 1. We know on general grounds that in a 2D system spin rotational symmetry can not be spontaneously broken at any finite temperature. However, this is not evident from the plot. The exponential growth of the spin-spin correlation length rapidly exceeds the size of the system and this creates the impression of long-range order at a finite temperature. One needs to carefully study the size dependence. The Binder ratios, defined in the appendix, prove useful for this purpose.

Figure 2 gives the spin binder ratios, g_S, which show no crossings with system size down to the lowest measured temperature, signifying absence of long range order at finite temperatures, in agreement with the Mermin-Wagner theorem. In contrast the orbital binder ratios g_n, shown in Fig. 3, have clear crossings at finite temperatures and we can extract T_c by comparing different system sizes. We obtain $T_c/J1 = 0.450 \pm 0.001$ for the isotropic spin-orbital model.

In Fig. 4 we show the scaling plot for the orbital susceptibility. The data collapse leads to estimates of critical

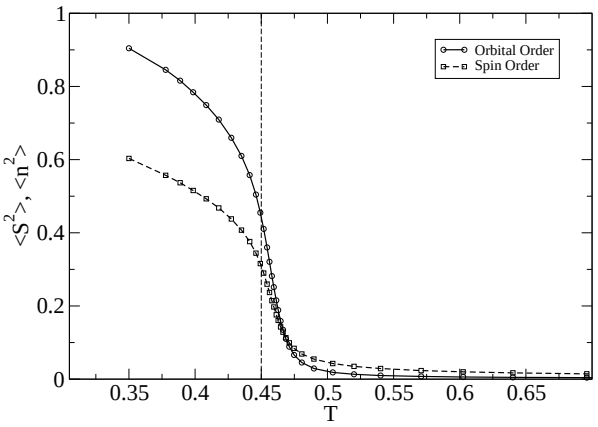

FIG. 1: Squares of spin and orbital order parameters as a function of temperature for the isotropic spin-orbital model on a 20×20 lattice. The vertical line shows the transition temperature T_c (measured in units of J_1), where the orbitals develop long-range order.

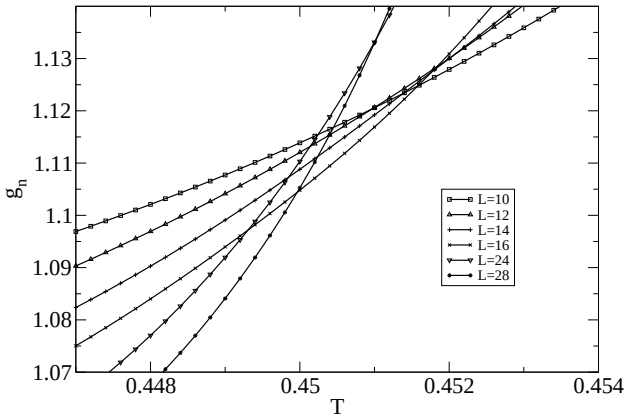

FIG. 3: Orbital Binder ratio as a function of temperature (measured in units of J_1) for different $L \times L$ lattices. In contrast to the spin variables, the discrete orbital variables undergo a phase transition, developing long range order at finite temperatures.

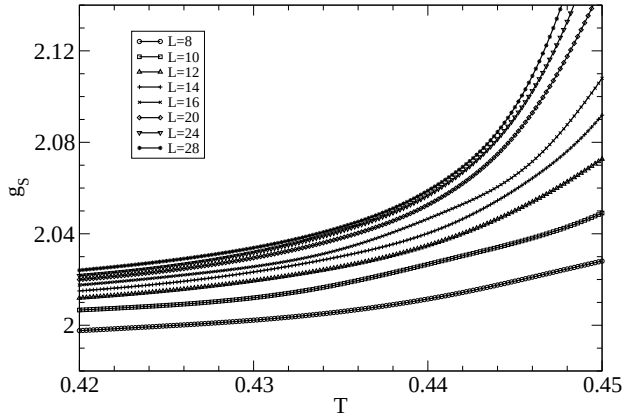

FIG. 2: Spin Binder ratio as a function of temperature (measured in units of J_1) for different $L \times L$ lattices. For the isotropic spin-orbital model there are no crossings in g_S at any temperatures of our simulation. This is consistent with the theory that in a 2D system there is no long range spin order at finite temperatures.

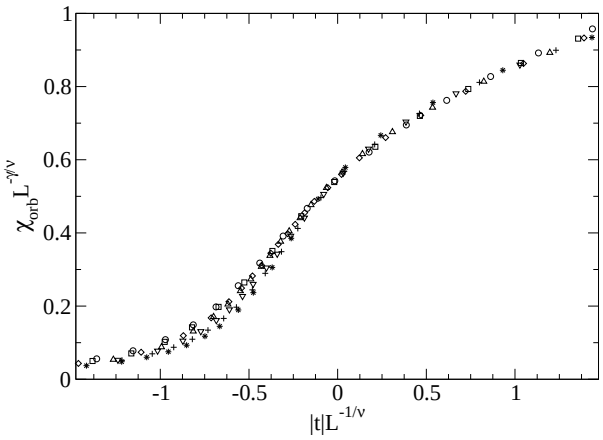

FIG. 4: The scaling of the universal $\tilde{\chi}$ versus reduced temperature $|t| = |(T - T_c)/T_c|$ shows that critical exponents are consistent with the 2D Ising Model.

exponents $\nu = 1.01 \pm .01$ and $\gamma = 1.75 \pm .02$. These exponents are consistent with the 2D Ising universality class. Figure 5 shows a plot of the specific heat, which grows rapidly near T_c. It is consistent with a logarithmic divergence but with an amplitude significantly larger than that in the pure 2D Ising model. The amplitude of the specific heat is not universal but is comparable for the Ising model on different 2D lattices.[75] It is considerably larger in our model, presumably as the Ising nematic variables associated with the spins couple directly to the orbitals and enhance the amplitude. We last note that the sharp peak in our specific heat clearly indicates a phase transition and its transition temperature T_c. Therefore, the Monte Carlo simulations of of our spin-orbital are less affected by finite-size effect compared to that in the frustrated square lattice J_1-J_2 model.[74]

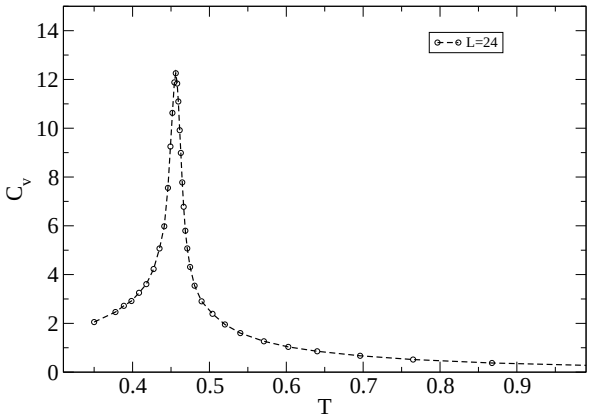

FIG. 5: Specific heat for the isotropic spin-orbital model under study. The sharp peak is consistent with a logarithmic divergence at T_c.

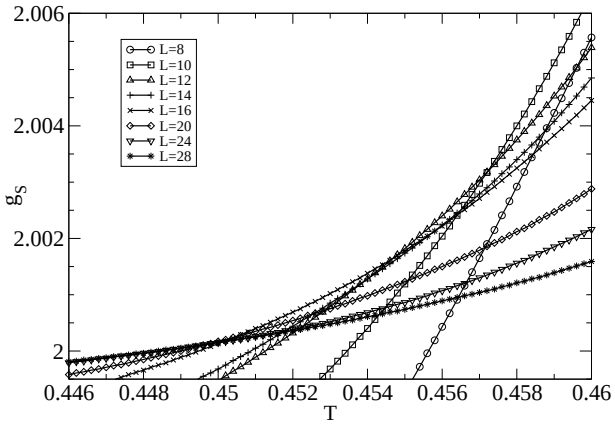

FIG. 6: Spin Binder ratio as a function of temperature (measured in units of J_1) for different $L\times L$ lattices. For anisotropic spins with either Ising or single ion anisotropy, finite spin ordering is observed besides orbital order.

B. Exchange and single-ion anisotropy

We next consider models with spin space anisotropy by generalizing the scalar product

$$\vec{S_i}\cdot\vec{S_j} = S_i^z S_j^z + \lambda[S_i^x S_j^x + S_i^y S_j^y] \ . \qquad (6)$$

We study the system for several values of the Ising anisotropy parameter λ. As long as $\lambda < 1$, there is only Ising symmetry for the spins, and both spins and orbitals can order at finite temperatures. The effect of the anisotropy on the orbital order is small, and the transition temperature is raised gradually as λ is reduced. In contrast, one can see a dramatic difference in the Binder ratios for the spin variables. Comparing to isotropic spins, viz. $\lambda = 1$, in Fig. 2, there are clear crossings in Fig. 6. We can extract T_c for both order parameters using the Binder ratio.

We summarize the extraction of T_c over a range of λ in Fig. 7. When λ is near (but not equal to) 1, we are in a regime where the spin transition temperature is non-zero but still separated from the orbital transition. However, when the anisotropy is small (in our case, $|1-\lambda| < 0.1$), computationally it is difficult to distinguish the two transitions. This shows that the spin transition temperature grows very rapidly with increasing anisotropy and it rapidly merges with the orbital transition. We note that with anisotropy the transition temperatures are within 10% of the mean-field value of $0.53J_1$.

We now introduce a single ion anisotropy, which is tied to orbital order.

$$H_{ion} = -D\sum_i^N (n_i S_i^{x\,2} + (1-n_i) S_i^{y\,2}) \ . \qquad (7)$$

In transition metal compounds, ligand crystal-field splitting lifts the degeneracy of the transition metal $3d$ orbitals, and the orbital angular moments are usually quenched. In this case, treating the relativistic spin-orbit coupling as a perturbation to the second order will result in a single-ion anisotropy term that reflects the underlying symmetry of the crystal. Therefore, an orthorhombic structural distortion or a net orbital polarization can lead to a single-ion anisotropy term closely tied to orbital order. This single ion anisotropy favors spin orientations along the AFM direction. One ordered configuration ob-

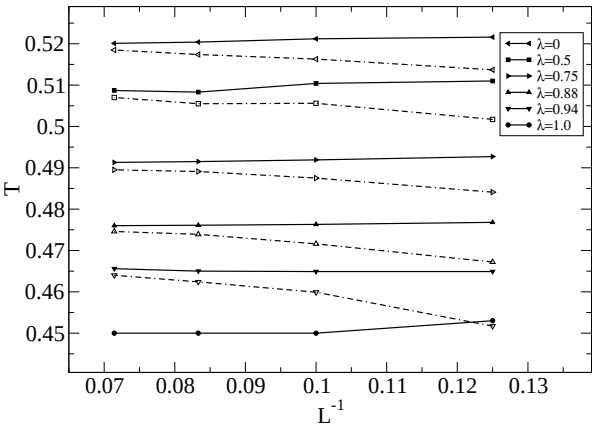

FIG. 7: From Binder cumulant ratios systematic crossings are located for systems of size L and $2L$. These are plotted versus inverse system length and extrapolated to get the thermodynamic T_c (measured in units of J_1). In all cases, the orbital crossings (solid) approach T_c from above and the spin crossings (dashed) approach it from below. For $\lambda = 1$, spins order only at zero temperature.

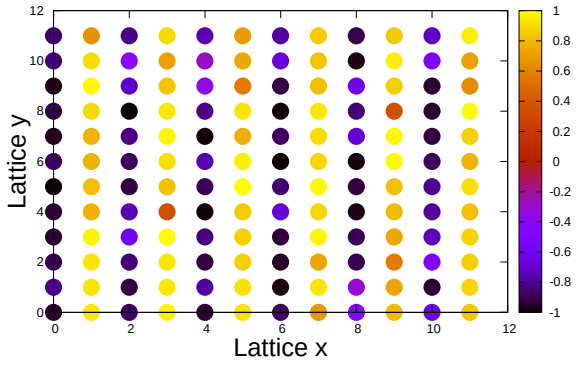

FIG. 8: In the orbital configuration $\{n_i = 1\}$, the spin-orbital model with single ion anisotropy has an AFM exchange along the x direction and favors the spin order collinear with this exchange. This is shown by plotting the S^x component from a typical spin configuration when in the $\{n_i = 1\}$ phase. The false color plot represents magnitude of the spin component along the x direction.

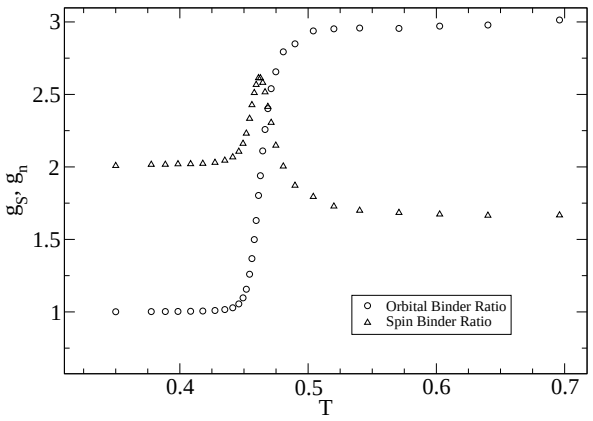

FIG. 9: For an isotropic ($\lambda = 1$) 24×24 system, we plot the orbital and spin binder ratios, g_n and g_S. g_n behaves smoothly between its limiting values while g_S develops what seems like a divergence at the transition temperature. The development of such an incipient divergence is an indicator of a first order transition.

served in the simulation is shown in Fig. 8.

Similar to the case of Ising-anisotropy (Eq. (6)), we have simulated these systems with different D values. For $|D| > 0.1$, once again we see no separation of the two ordering transitions for spins and orbitals. This shows that, like the Ising anisotropy, the uniaxial anisotropy causes a rapid increase in the spin ordering temperature and it soon merges with the orbital order.

In Fig. 9, we show the binder ratios for orbitals and spins. Binder ratios for orbitals remain well behaved regardless of the anisotropy introduced in the models. However, there is a clear incipient divergence in g_S, which is indicative of a first order transition. In general, we find that the spins have a greater tendency for a first order transition than the orbitals. The implications of these results for the pnictides are discussed in the next section.

IV. V. DISCUSSION AND RELEVANCE TO THE IRON PNICTIDES

In this section, we use the results of Monte Carlo simulations, mean field theory and general arguments about quasi-2D spin systems to develop an overall phase-diagram for coupled spin-orbital systems. We will then explore the applicability of the phase diagram to the iron-pnictide materials. The key issues of interest to us are whether there is a single transition or two separate transitions, and whether each of the transitions is first or second order.

A. The phase diagram of the spin-orbital model

The mean-field theory gives a simultaneous spin and orbital transition, which could be first or second order depending on the exchange couplings. Monte Carlo simulations show that the spin and orbital transitions are practically simultaneous unless the spin space anisotropy is very small. In the latter case, divergent long-wavelength fluctuations push the spin transition temperature to zero, whereas the orbital transition is not significantly affected by these fluctuations. The transition temperatures observed in the simulations are within a few percent of the mean-field value of $0.53J_1$ when the anisotropy is large. As the anisotropy goes to zero, the orbital transition is reduced by less than 20%, whereas the spin transition is reduced all the way to zero. Even a 5% anisotropy causes a near simultaneous transition.

On general grounds, one knows that in place of long-range order the correlation length in a 2D Heisenberg spin system stays finite but grows exponentially as $\exp C/T$ as the temperature is lowered. This implies that if below some energy scale ϵ_0 these divergent fluctuations are cut off (due to for example spin space anisotropy or 3D coupling), it will lead to long-range order and the transition temperature will depend on the energy scale as $1/\ln(\epsilon_0/\epsilon)$, rising very steeply with increasing ϵ.[72] Our Monte Carlo simulations show that unless the spin transition is significantly suppressed by fluctuations the spin and orbital transitions would happen together.

The simulation results also show that the isolated orbital transition is in the universality class of the 2D Ising model. While we have not been able to observe the isolated finite temperature spin transition when it is separated from the orbital transition, on general grounds, we expect it also to be a continuous transition in the univer-

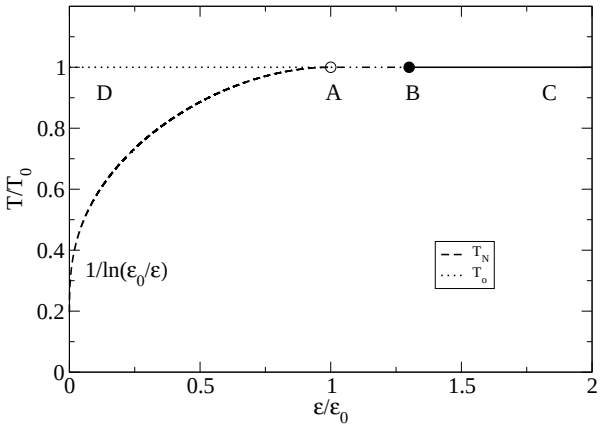

FIG. 10: Phenomenological phase diagram for the spin-orbital model. The exchange energy scale in the problem sets the transition temperature T_O for orbital order, which in turn drives the structural transition. ϵ_0 is the energy scale below which long wavelength fluctuations are suppressed. There are two separate continuous orbital and magnetic transitions for $\epsilon \ll \epsilon_0$ (shown as dotted and dashd lines respectively) and one simultaneous first order transition for $\epsilon \gg \epsilon_0$ (shown as a solid line). Near the region $\epsilon \simeq \epsilon_0$ (segment AB in the figure), the two transition temperatures can be very close and can be continuous or first order. In iron pnictides, ϵ would refer to the larger of the spin anisotropies or 3D couplings.

sality class of the 2D Ising model (due to a small but non-zero spin space anisotropy). If the 3D couplings are more important than spin space anisotropy, then the transition could have a significant crossover region in the universality class of the 3D Heisenberg model (but will ultimately be in the 3D Ising universality class if a uniaxial spin anisotropy is also present). When the two transitions come together, the simulations find that the transitions tend to become first order.

Based on the above, we propose a phenomenological phase diagram (See Fig. 10) with the following features:

1. The structural transition is driven by orbital ordering, which happens at temperature T_O. It is set by the exchange energy scale in the problem.

2. Let ϵ_0 be the energy scale below which the long-wavelength fluctuations are suppressed. Then the ratio of Neel to orbital transition can be parametrized as ($x = \epsilon/\epsilon_0$)

$$\frac{T_N}{T_O} = \frac{2-x}{1+\ln 1/x} \qquad for\ x \ll 1, \tag{8}$$

and,

$$T_N/T_O = 1 \qquad for\ x \gg 1. \tag{9}$$

We have two continuous phase transitions for $x \ll 1$ and one simultaneous first order transition for $x \gg 1$. In between, the region $x \simeq 1$ can have a small stretch where the two transitions are practically inseparable but remain continuous (AB in Fig. 10). The two transitions merge into a first order transition at the point B in Fig. 10.

We last note that in principle, doping can be the source of another kind of additional fluctuation which significantly reduces both spin and orbital transition temperatures from the mean-field values. This can also lead to the separation of structural and magnetic transition as observed in many families of iron pnictides.

B. Discussion of materials

We next discuss the relevance of this study to various experimental findings in the iron-pnictide materials.

As mentioned previously, the parent compounds of the 1111 family have two separate second order phase transitions, while in the 122 family the two transitions are closer to each other in temperature. In the undoped $BaFe_2As_2$, the two transitions are slightly separated, where the structural transition starts as second order and is followed by a simultaneous first order jump both in the lattice distortion and magnetic transition at a lower temperature.[39–41] On the other hand, in $CaFe_2As_2$ and $SrFe_2As_2$ the structural and magnetic phase transitions happen together as a single first order transition.[42–44]

The three behaviors reported in different iron-pnictide materials are all captured by our phase diagram of a coupled spin-orbital Hamiltonian. In particular, phase transitions in the 1111 family correspond to the case when ϵ is small and away from ϵ_0, where the structural and magnetic phase transitions are separated and of second order. On the other hand, phase transitions of $CaFe_2As_2$ and $SrFe_2As_2$ correspond to the case when ϵ is much larger than ϵ_0, where the two transitions occur as a single first order transition. The region $\epsilon \simeq \epsilon_0$ is relevant to $BaFe_2As_2$. In this case, the structural and magnetic transition temperatures can be very close and there is a tendency for the magnetic transition to become first order. This indicates that these materials are close to the boundary between the distinct regions.

One can further ask which interaction term controls ϵ in the iron-pnictide materials. In this study we have investigated the role of spin space anisotropies described by Eq. (6) or Eq. (7). Their effects on the transition temperature are in essence the same as exchange couplings in the third direction.[38,51,53] Phenomenologically, ϵ would refer to the larger of the terms in determining the phase transitions. It is known that the 122 family is more disperse in the third direction than the 1111 family. In particular, in the 122 family spin-wave spectra from neutron scattering are usually fitted with an additional 3D exchange coupling J_c, while for the 1111 materials J_c is essentially zero. In $BaFe_2As_2$, the third-direction coupling is non-zero but also appears small; the reported J_c/J_1 is roughly 1%.[77,78] Since a 2D Ising universality has been found for this material,[76] a uniaxial spin anisotropy could be more important. On the other

hand, in $CaFe_2As_2$ and $SrFe_2As_2$, J_c is more substantial and J_c/J_1 is estimated to be 10%.[22,79] Therefore, in these materials spin exchange coupling in the third direction could be the controlling factor for ϵ.

We note that coupling to other degrees of freedom such as the lattice variable could also turn the isolated orbital or magnetic transition into first order. However, besides the phase diagram, the orbital variables have proven indispensable in describing various other properties of iron-based superconductors such as the emergent transport anisotropies.[23–27,81,82]

A modest orbital polarization has been reported by angle-resolved photoemission (ARPES) experiments performed on the 122 family of iron pnictide materials.[33–36] This observation is crucial in explaining the striking phenomenon that in these materials the resistivity is smaller in the longer AFM axis.[23–27] This unexpected behavior is striking especially because optical measurements indicate a smaller scattering rate along the shortened FM direction.[28,29] It is the presence of an anisotropic effective mass due to a preferred occupation of d_{xz} over d_{yz} orbitals on the Fermi level that renders a better conducting pathway along the AFM direction.[81,82]

As mentioned previously, with a preferential occupation of d_{xz} orbitals over d_{yz} orbitals, relativistic spin-orbit coupling can induce an orbital angular momentum in the xy plane and lead to a single ion anisotropy. An excess population of d_{xz} orbitals (through an induced $d_{xz}+id_{xy}$ piece) can favor spins to point along the x-axis while excess population of d_{yz} orbitals can favor spins to point along the y direction. We propose that this mechanism is the reason why the observed directions of ordered spin moments are tied to antiferromagnetism and end up point along the AFM direction.

We last note that a possible orbital ordering has also been proposed for $Fe_{1+y}Te_xSe_{1-x}$ (the so-called 11 family of iron chalcogenides).[83,84]. In these materials, the ordered moments form a $(\pi/2, \pi/2)$ diagonal double stripe pattern, and the spin orientation points toward the *FM direction*.[85,86] Based on our discussion above, we believe this implies on the Fermi level a preferred population of Wannier functions whose orbital lobes point along the same direction. One direct consequence of this prediction is that *in 11 iron chalcogenides resistivity is smaller in the FM direction*.[84,87] This is indeed consistent with recent resistivity measurements.[88] The above prediction could be further tested by future ARPES and optical experiments on de-twinned iron chalcogenides.

V. CONCLUSION

In summary, we have studied finite-temperature phase transitions in a Hamiltonian of coupled Heisenberg spin and Ising orbital degrees of freedom. Using mean-field theory, Monte Carlo simulations, and general arguments we established the phase diagram of such a spin-orbital model and discussed its relevance to the iron-pnictide superconductors. We found that if spin rotational invariance is preserved, the magnetic transition temperature is pushed to zero in accord with the Mermin-Wagner theorem. In this case, there is only one single finite-temperature orbital phase transition which belongs to the 2D Ising universality class. By introducing spin space anisotropies into the Hamiltonian, spins can order at finite temperatures and the magnetic and orbital transitions are found to couple together and become first order. This phase diagram captures several observed behaviors in the 1111 and 122 families of iron pnictides. We also studied the case when relativistic spin-orbit coupling leads to a uniaxial anisotropy and found that the preferred spin-orientation is driven by orbital order. This explains why the direction of ordered moment in these materials is tied to their antiferromagnetism.

In the field of iron-based superconductors, there are several open questions that remain to be answered. It is interesting to further explore other experimental implications of model Hamiltonians with coupled spin and orbital degrees of freedom. For example, can fluctuations in orbital and/or spin variables account for various anomalous phenomena that occur above the structural and magnetic transition temperatures?[89] What are the effects of orbital order and orbital fluctuations on twin boundaries? Are they related to the enhanced superconductivity at domain walls in these materials?[90,91] Calculations to address these interesting open questions are areas of future study.

acknowledgments

The authors acknowledge discussions with N. Curro, J.-H. Chu, I. R. Fihser, R. Thomale, A. Diougardi, W. Pickett, R. M. Fernandes, and Y. Kamiya. R.A. and R.R.P.S. are supported by NSF Grant No. DMR-1004231. C.C.C. and T.P.D. are supported by the U.S. DOE under Contract No. DE-AC02-76SF00515.

[1] Y. Kamihara, T. Watanabe, M. Hirano, and H. Hosono, J. Am. chem. Soc. **130**, 3296 (2008).
[2] M. Rotter, M. Tegel, and D. Johrendt, Phys. Rev. Lett. **101**, 107006 (2008).
[3] D. C. Johnston, Adv. Phys. **59**, 803 (2010).
[4] J. Zhao, Q. Huang, C. de la Cruz, S. Li, J. W. Lynn, Y. Chen, M. A. Green, G. F. Chen, G. Li, Z. Li, J. L. Luo, N. L. Wang, and P. Dai, Nature Mater. **7**, 953 (2008).
[5] C. R. Rotundu, D. T. Keane, B. Freelon, S. D. Wilson, A. Kim, P. N. Valdivia, E. Bourret-Courchesne, and R. J. Birgeneau, Phys. Rev. B **80**, 144517 (2009).
[6] M. A. McGuire, A. D. Christianson, A. S. Sefat, B. C. Sales, M. D. Lumsden, R. Jin, E. Andrew Payzant, D. Mandrus, Y. Luan, V. Keppens, V. Varadarajan, J. W. Brill, R. P. Hermann, M. T. Sougrati, F. Grandjean, and G. J. Long, Phys. Rev. B **78**, 094517.
[7] H. Chen, Y. Ren, Y. Qiu, W. Bao, R. H. Liu, G. Wu, T. Wu, Y. L. Xie, X. F. Wang, Q. Huang, and X. H. Chen, Euro. Phys. Lett. **85**, 17006 (2009).
[8] J.-H. Chu, J. G. Analytis, C. Kucharczyk, and I. R. Fisher, Phys. Rev. B **79**, 014506 (2009).
[9] S. Nandi, M. G. Kim, A. Kreyssig, R. M. Fernandes, D. K. Pratt, A. Thaler, N. Ni, S. L. Budko, P. C. Canfield, J. Schmalian, R. J. McQueeney, and A. I. Goldman, Phys. Rev. Lett **104**, 057006 (2010).
[10] C. de la Cruz, Q. Huang, J. W. Lynn, J. Li, W. Ratcliff II, J. L. Zarestky, H. A. Mook, G. F. Chen, J. L. Luo, N. L. Wang, and P. Dai, Nature **453**, 89 (2008).
[11] Y. Chen, J. W. Lynn, J. Li, G. Li, G. F. Chen, J. L. Luo, N. L. Wang, P. Dai, C. dela Cruz, and H. A. Mook, Phys. Rev. B **78**, 064515 (2008).
[12] J. Zhao, Q. Huang, C. de la Cruz, J. W. Lynn, M. D. Lumsden, Z. A. Ren, J. Yang, X. Shen, X. Dong, Z. Zhao, and P. Dai, Phys. Rev. B **78**, 132504 (2008).
[13] Q. Huang, Y. Qiu, Wei Bao, M. A. Green, J. W. Lynn, Y. C. Gasparovic, T. Wu, G. Wu, and X. H. Chen, Phys. Rev. Lett. **101**, 257003 (2008).
[14] M. Kofu, Y. Qiu, W. Bao, S.-H. Lee, S. Chang, T. Wu, G. Wu, and X. H. Chen, New J. Phys. **11**, 055001 (2009).
[15] Y. Su, P. Link, A. Schneidewind, Th. Wolf, P. Adelmann, Y. Xiao, M. Meven, R. Mittal, M. Rotter, D. Johrendt, Th. Brueckel, and M. Loewenhaupt, Phys. Rev. B **79**, 064504 (2009).
[16] A. I. Goldman, D. N. Argyriou, B. Ouladdiaf, T. Chatterji, A. Kreyssig, S. Nandi, N. Ni, S. L. Budko, P. C. Canfield, and R. J. McQueeney, Phys. Rev. B **78**, 100506(R) (2008).
[17] K. Kaneko, A. Hoser, N. Caroca-Canales, A. Jesche, C. Krellner, O. Stockert, and C. Geibel, Phys. Rev. B **78**, 212502 (2008).
[18] Jun Zhao, W. Ratcliff, II, J. W. Lynn, G. F. Chen, J. L. Luo, N. L. Wang, J. P. Hu, and P. Dai, Phys. Rev. B **78**, 140504(R) (2008).
[19] M. D. Lumsden and A. D. Christianson, J. Phys.: Condens. Matter **22**, 203203 (2010).
[20] J. Zhao, D. T. Adroja, D.-X. Yao, R. Bewley, S. Li, X. F. Wang, G. Wu, X. H. Chen, J. P. Hu, and P. Dai, Nature Physics **5** 555 (2009).
[21] R. A. Ewings, T. G. Perring, R. I. Bewley, T. Guidi, M. J. Pitcher, D. R. Parker, S. J. Clarke, and A. T. Boothroyd, Phys. Rev. B **78**, 220501(R) (2008).
[22] R. A. Ewings, T. G. Perring, J. Gillett, S. D. Das, S. E. Sebastian, A. E. Taylor, T. Guidi, and A. T. Boothroyd4, Phys. Rev. B **83**, 214519 (2011).
[23] J.-H. Chu, J. G. Analytis, D. Press, K. De Greve, T. D. Ladd, Y. Yamamoto, and I. R. Fisher, Phys. Rev. B **81**, 214502 (2010).
[24] J.-H. Chu, J. G. Analytis, K. De Greve, P. L. McMahon, Z. Islam, Y. Yamamoto, and I. R. Fisher, Science **329**, 824 (2010).
[25] M. A. Tanatar, E. C. Blomberg, A. Kreyssig, M. G. Kim, N. Ni, A. Thaler, S. L. Budko, P. C. Canfield, A. I. Goldman, I. I. Mazin, and R. Prozorov, Phys. Rev. B **81**, 184508 (2010).
[26] J. J. Ying, X. F. Wang, T. Wu, Z. J. Xiang, R. H. Liu, Y. J. Yan, A. F. Wang, M. Zhang, G. J. Ye, P. Cheng, J. P. Hu, and X. H. Chen, Phys. Rev. Lett. **107**, 067001 (2011).
[27] H.-H. Kuo, J.-H. Chu, S. C. Riggs, L. Yu, P. L. McMahon, K. D. Greve, Y. Yamamoto, J. G. Analytis, and I. R. Fisher, Phys. Rev. B **84**, 054540 (2011).
[28] A. Dusza, A. Lucarelli, F. Pfuner, J.-H. Chu, I. R. Fisher, and L. Degiorgi, Euro Phys. Lett. **93**, 37002 (2011).
[29] A. Lucarelli, A. Dusza, A. Sanna, S. Massidda, J.-H. Chu, I.R. Fisher, and L. Degiorgi, arXiv:11087.0670.
[30] M. Nakajima, T. Liang, S. Ishida, Y. Tomioka, K. Kihou, C. H. Lee, A. Iyo, H. Eisaki, T. Kakeshita, T. Ito, and S. Uchida, ,PNAS **108**, 12238 (2011).
[31] T.-M. Chuang, M. P. Allan, J. Lee, Y. Xie, Ni Ni, S. L. Budko, G. S. Boebinger, P. C. Canfield, and J. C. Davis, Science **327**, 181 (2010).
[32] I. R. Fisher, L. Degiorgi, and Z. X. Shen, Rep. Prog. Phys. **74**, 124506 (2011).
[33] T. Shimojima, K. Ishizaka, Y. Ishida, N. Katayama, K. Ohgushi, T. Kiss, M. Okawa, T. Togashi, X.-Y. Wang, C.-T. Chen, S. Watanabe, R. Kadota, T. Oguchi, A. Chainani, and S. Shin, Phys. Rev. Lett. **104**, 057002 (2010).
[34] S.-H. Lee, G. Xu, W. Ku, J. S. Wen, C. C. Lee, N. Katayama, Z. J. Xu, S. Ji, Z. W. Lin, G. D. Gu, H.-B. Yang, P. D. Johnson, Z.-H. Pan, T. Valla, M. Fujita, T. J. Sato, S. Chang, K. Yamada, and J. M. Tranquada, Phys. Rev. B **81**, 220502(R) (2010).
[35] Q. Wang, Z. Sun, E. Rotenberg, F. Ronning, E. D. Bauer, H. Lin, R. S. Markiewicz, M. Lindroos, B. Barbiellini, A. Bansil, D. S. Dessau, arXiv:1009.0271.
[36] M. Yi, D. Lu, J.-H. Chu, J. G. Analytis, A. P. Sorini, A. F. Kemper, B. Moritz, S.-K. Mo, R. G. Moore, M. Hashimoto, W.-S. Lee, Z. Hussain, T. P. Devereaux, I. R. Fisher, and Z.-X. Shen, PNAS **108**, 17 (2011).
[37] Q. Si and E. Abrahams, Phys. Rev. Lett. **101**, 076401 (2008).
[38] C. Fang, H. Yao, W.-F. Tsai, J. P. Hu, and S. A. Kivelson, Phys. Rev. B **77** 224509 (2008).
[39] C. R. Rotundu, B. Freelon, T. R. Forrest, S. D. Wilson, P. N. Valdivia, G. Pinuellas, A. Kim, J.-W. Kim, Z. Islam, E. Bourret-Courchesne, N. E. Phillips, and R. J. Birgeneau, Phys. Rev. B **82**, 144525 (2010).
[40] M. G. Kim, R. M. Fernandes, A. Kreyssig, J. W. Kim, A. Thaler, S. L. Budko, P. C. Canfield, R. J. McQueeney, J. Schmalian, and A. I. Goldman, Phys. Rev. B **83**, 134522 (2011).
[41] C. R. Rotundu and R. J. Birgeneau, arXiv:1106.5761.
[42] N. Ni, S. Nandi, A. Kreyssig, A. I. Goldman, E. D. Mun, S. L. Budko, and P. C. Canfield, Phys. Rev. B **78**, 014523

(2008).
[43] J.-Q. Yan, A. Kreyssig, S. Nandi, N. Ni, S. L. Budko, A. Kracher, R. J. McQueeney, R. W. McCallum, T. A. Lograsso, A. I. Goldman, and P. C. Canfield, Phys. Rev. B **78**, 024516 (2008).
[44] J. Gillett, S. D. Das, P. Syers, A. K. T. Ming, J. I. Espeso, C. M. Petrone, and S. E. Sebastian, arXiv:1005.1330.
[45] T. Yildirim, Phys. Rev. Lett. **101**, 057010 (2008).
[46] C. Xu, M. Mueller and S. Sachdev, Phys. Rev. B **78**, 020501 (2008).
[47] K. Haule, J. H. Shim, and G. Kotliar, Phys. Rev. Lett. **100**, 226402 (2008).
[48] I. I. Mazin and M. D. Johannes, Nat. Phys. **5**, 141 (2009).
[49] Z. P. Yin S. Lebégue, M. J. Han, B. P. Neal, S. Y. Savrasov, and W. E. Pickett, Phys. Rev. Lett. **101**, 047001 (2008).
[50] M. J. Han, Q. Yin, W. E. Pickett, and S. Y. Savrasov, Phys. Rev. Lett. **102**, 107003 (2009).
[51] A. L. Wysocki, K. D. Belashchenko, and V. P. Antropov, Nature Physics **7**, 485 (2011).
[52] D. Stanek, O. P. Sushkov, and G. S. Uhrig, Phys. Rev. B **84**, 064505 (2011).
[53] Y. Kamiya *et al.*, arXiv:arXiv:1108.1599.
[54] F. Krüger, S. Kumar, J. Zaanen, and J. van den Brink, Phys. Rev. B **79**, 054504 (2009).
[55] R. R. P. Singh, arXiv:0903.4408.
[56] C.-C. Chen, B. Moritz, J. van den Brink, T. P. Devereaux, and R. R. P. Singh, Phys. Rev. B **80**, 180418(R) (2009).
[57] W. Lv, J. Wu, and P. Phillips, Phys. Rev. B **80**, 224506 (2009); W. Lv, F. Kruger and P. Phillips, Phys. Rev. B 82, 045125 (2010).
[58] C.-C. Lee , W.-G. Yin, and W. Ku, Phys. Rev. Lett. **103**, 267001 (2009).
[59] K .Kubo and P. Thalmeier, J. Phys. Soc. Jpn. **78**, 083704 (2009).
[60] Y. Yanagi, Y. Yamakawa, N. Adachi, and Y. Ono, J. Phys. Soc. Jpn. **79**, 123707 (2010).
[61] E. Bascones, M. J. Calderoń, and B. Valenzuela, Phys. Rev. Lett. **104**, 227001 (20100.
[62] H. Kontani, T. Saito, and S. Onari, Phys. Rev. B **84**, 024528 (2011).
[63] A. H. Nevidomskyy, arXiv:1104.1747.
[64] R. M. Fernandes, L. H. VanBebber, S. Bhattacharya, P. Chandra, V. Keppens, D. Mandrus, M. A. McGuire, B. C. Sales, A. S. Sefat, and J. Schmalian, Phys. Rev. Lett. **105**, 157003 (2010).
[65] I. Paul, Phys. Rev. Lett. **107**, 047004 (2011).
[66] V. Cvetkovic and Z. Tesanovic, Euro. Phys. Lett. **85**, 37002 (2009).
[67] J. Knolle, I. Eremin, A. V. Chubukov, and R. Moessner, Phys. Rev. B **81**, 140506(R) (2010).
[68] P. M. R. Brydon and C. Timm, Phys. Rev. B **79**, 180504(R) (2009).
[69] H. Zhai, F. Wang, and D.-H. Lee, Phys. Rev. B **80**, 064517 (2009).
[70] R. M. Fernandes *et al.*, arXiv:1110.1893.
[71] K. I. Kugel and D. I. Khomskii, Sov. Phys. Usp. **25**, 231 (1982).
[72] S. Chakravarty. B. I. Halperin and D. R. Nelson, Phys. Rev. B **39**, 2344 (1989).
[73] R. Applegate, R. R. P. Singh, and J. Oitmaa, Phys. Rev. B **81**, 024505 (2010).
[74] C. Weber *et al.*, Phys. Rev. Lett. **91**, 177202 (2003).
[75] R. M. F. Houtappel, Physica 16, 425 (1950).
[76] S. D. Wilson, C. R. Rotundu, Z. Yamani, P. N. Valdivia, B. Freelon, E. Bourret-Courchesne and R. J. Birgeneau, Phys. Rev. B **81**, 014501 (2010).
[77] K. Matan, R. Morinaga, K. Iida, and T. J. Sato, Phys. Rev. B **79**, 054526 (2009).
[78] A. D. Christianson, M. D. Lumsden, S. E. Nagler, G. J. MacDougall, M. A. McGuire, A. S. Sefat, R. Jin, B. C. Sales, and D. Mandrus, Phys. Rev. Lett. **103**, 087002 (2009).
[79] S. O. Diallo, V. P. Antropov, T. G. Perring, C. Broholm, J. J. Pulikkotil, N. Ni, S. L. Budko, P. C. Canfield, A. Kreyssig, A. I. Goldman, and R. J. McQueeney, Phys. Rev. Lett. **102**, 187206 (2009).
[80] A. Cano, M. Civelli, I. Eremin, and I. Paul, Phys. Rev. B **82**, 020408(R) (2010).
[81] C.-C. Chen, J. Maciejko, A. P. Sorini, B. Moritz, R. R. P. Singh, and T. P. Devereaux, Phys. Rev. B **82**, 100504(R) (2010).
[82] W. Lv and P. Phillips, arXiv:1105.4630.
[83] F.-C. Hsu, J.-Y. Luo, K.-W. Yeh, T.-K. Chen, T.-W. Huang, P. M. Wu, Y.-C. Lee, Y.-L. Huang, Y.-Y. Chu, D.-C. Yan, and M.-K. Wu, PNAS **105**, 14262 (2008).
[84] A. M. Turner, F. Wang, and A. Vishwanath, Phys. Rev. B **80**, 224504 (2009).
[85] W. Bao, Y. Qiu, Q. Huang, M. A. Green, P. Zajdel, M. R. Fitzsimmons, M. Zhernenkov, S. Chang, M. Fang, B. Qian, E. K. Vehstedt, J. Yang, H. M. Pham, L. Spinu, and Z. Q. Mao, Phys. Rev. Lett. **102**, 247001 (2009).
[86] S. Li, C. de la Cruz, Q. Huang, Y. Chen, J. W. Lynn, J. P. Hu, Y.-L. Huang, F.-C. Hsu, K.-W. Yeh, M.-K. Wu, and P. Dai, Phys. Rev. B **79**, 054503 (2009).
[87] L. Hao, C.-C. Lee, and T. K. Lee, arXiv:1107.1952.
[88] J.-H. Chu, private communication.
[89] H. Z. Arham, C. R. Hunt, W. K. Park, J. Gillett, S. D. Das, S. E. Sebastian, Z. J. Xu, J. S. Wen, Z. W. Lin, Q. Li, G. Gu, A. Thaler, S. L. Budko, P. C. Canfield, and L. H. Greene, arXiv:1108.2749.
[90] B. Kalisky, J. R. Kirtley, J. G. Analytis, Jiun-Haw Chu, A. Vailionis, I. R. Fisher, and K. A. Moler, Phys. Rev. B **81**, 184513 (2010).
[91] H. Xiao, T. Hu, A. P. Dioguardi, N. Roberts-Warren, A. C. Shockley, J. Crocker, Z. Viskadourakis, X. Y. Tee, I. Radulov, C. C. Almasan, N. J. Curro, and C. Panagopoulos, arXiv:1107.0904.
[92] K. Hukushima and K. Nemoto, J. Phys. Soc. Jpn. **65**, 1604 (1996).
[93] H. G. Katzgraber, S. Trebst, D. A. Huse, and M. Troyer, J. Stat. Mech. P03018 (2006).
[94] D. J. Earl and M. W. Deem, arXiv:physics/0508111.
[95] S. Trebst, D. A. Huse, and M. Troyer, Phys. Rev. E **70**, 046701 (2004).
[96] L. Wang, K. S. D. Beach, A. W. Sandvik, Phys. Rev. B **73**, 014431 (2006).
[97] M. S. S. Challa, D. P. Landau, and K. Binder, Phys. Rev B **34** 18411852 (1986).

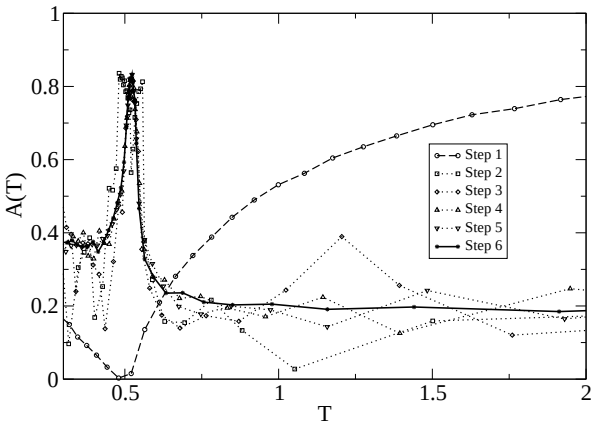

FIG. 11: The acceptance probability is plotted versus temperature for several feedback steps. The initial geometric distribution shows a pronounced dip in acceptance near the critical point and later feedback steps show how this is corrected by clustering replicas around T_c.

VI. APPENDIX

A. Monte Carlo Simulations with Parallel Tempering

We have used a parallel tempering Exchange Monte Carlo (EMC) method to simulate our models.[92,93] It is an efficient extended ensemble simulation method that simulates multiple copies (replicas) of the system simultaneously at different temperatures. Exchanges between replica configurations are accepted or rejected in accordance with detailed balance. Replica exchange has been used to study systems spanning many fields including strongly correlated systems, biological pathways, and spin glasses.[94] The advantage of these methods is that while at high temperatures the system's memory is erased and when replicas go back to lower temperatures they explore large phase space uncorrelated in monte carlo time.[95]

Recently, Katzgraber et al.[93] showed that in order to maximally benefit from EMC, the temperature distribution must be determined in a nontrivial way via a "feedback" method. The temperature distribution $\{T_i\}$ is obtained by starting with some initial set and recording statistics on the "round trip" time from T_{low} to T_{high}. Minimization of this round trip time results in the optimal distribution. The endpoints, $\{T_{low}...T_{high}\}$ are fixed and feedbacks of the simulation are done until the distribution converges. The evolution of acceptance probability is shown in Fig. 11. Once $\{T_i\}$ is determined, an exchange monte carlo simulation is performed using the stored optimal temperature distribution.

Between the EMC moves that exchange replicas, one has some freedom in how to update each individual replica, provided one can always know the energy of that replica. We choose to do local spin/orbital flips by sweeping over the lattice and randomly choosing whether or not a site in the lattice attempts a spin flip or an orbital flip.

B. Orbital and Spin Measurements

There are two order parameters of interest for our Hamiltonian, one associated with the orbital degrees of freedom and another with the spin degrees of freedom. We measure second and fourth moments for both variables, and, in the case of the magnetization, we measure at the two AFM wave vectors of interest, $\vec{Q}_1 = (\pi, 0)$, and $\vec{Q}_2 = (0, \pi)$.

$$\langle n^2 \rangle = \langle \left((\frac{1}{N}\sum_i^N n_i) - \langle n \rangle \right)^2 \rangle \tag{10}$$

$$\langle n^4 \rangle = \langle \left((\frac{1}{N}\sum_i^N n_i) - \langle n \rangle \right)^4 \rangle \tag{11}$$

$$\langle S^2 \rangle = \langle \left(\frac{1}{N}\sum_i^N \vec{S}_i e^{i\vec{Q}\cdot\vec{r}_i} \right)^2 \rangle \tag{12}$$

$$\langle S^4 \rangle = \langle \left(\frac{1}{N}\sum_i^N \vec{S}_i e^{i\vec{Q}\cdot\vec{r}_i} \right)^4 \rangle \tag{13}$$

The n_i take value 0 or 1 in our model and $\langle n \rangle = \frac{1}{2}$. The S_i are classical Heisenberg spins with magnitude unity and $\langle \vec{S} \rangle = 0$. These orbital and spin measurements are used to evaluate Binder cumulant ratios as discussed below.

C. Binder Ratios

We define the Binder ratios for the orbitals g_n and for the spins g_S through the relations:

$$g_n = \frac{\langle n^4 \rangle}{\langle n^2 \rangle^2} \tag{14}$$

$$g_S = \frac{\langle S^4 \rangle}{\langle S^2 \rangle^2}. \tag{15}$$

At low temperatures, the spin and orbital order parameter distributions will be sharply peaked at their extremum values. At high temperatures all variables will have gaussian distributions. For $T \ll T_c$ the orbital quantities are:

$$\langle n^2 \rangle = \frac{1}{4} \tag{16}$$

$$\langle n^4 \rangle = \frac{1}{16} \tag{17}$$

$$g_n = 1\ . \tag{18}$$

For the spins, the low temperature limits are

$$\langle S^2 \rangle = \frac{3}{2} \tag{19}$$

$$\langle S^4 \rangle = \frac{9}{2} \tag{20}$$

$$g_S = 2 \tag{21}$$

The two orbital orders divide the system between Q_1 and Q_2, resulting in different limits than a system without competing ordering wave vectors.

At high temperature, $T \gg T_c$, we get well known results for the Binder ratio:

$$\langle n^2 \rangle = 1 \tag{22}$$

$$\langle n^4 \rangle = 3 \tag{23}$$

$$g_n = 3 \tag{24}$$

$$\langle S^2 \rangle = 3 \tag{25}$$

$$\langle S^4 \rangle = 15 \tag{26}$$

$$g_S = \frac{5}{3} \tag{27}$$

The difference between orbitals and spins comes purely from the dimensionality of the variable. We note that for g_S, in contrast to the low temperature limits, the high temperature limits do not depend on the presence two ordering wavevectors.

D. First and Second Order Phase Transitions

We can estimate the thermodynamic T_c by carefully studying the size dependence of various physical quantities. We rely on the Binder ratios defined previously and well known finite size scaling arguments to address the types of transitions we measure. We propose the usual scaling ansatz for the susceptibility,

$$t = \frac{T - T_c}{T_c} \tag{28}$$

$$\chi(t, L) = L^{\frac{\gamma}{\nu}} \tilde{\chi}(L^{\frac{1}{\nu}}|t|). \tag{29}$$

t is the reduced temperature, and $\chi(t, L)$ is the susceptibility per spin for a system of size L. $\tilde{\chi}$ is some unknown but universal function and ν and γ are critical exponents which denote the power law divergence at T_c.

The Binder ratios g_n and g_S have the property that at T_c, they are independent of system size, universal constants of the system. We find T_c from Binder Ratio measurements for many pairs of systems of size L and $2L$ and plotting versus temperature. A crossing for a given pair gives a constant and T_c. Size dependence of this constant exponentially decays versus the system size.[96] A more prominent size dependence occurs for the spins than orbitals in Fig. 7. We extrapolate the size dependence to large L by fitting the exponential decay. The y-intercept of this fit is the thermodynamic T_c.

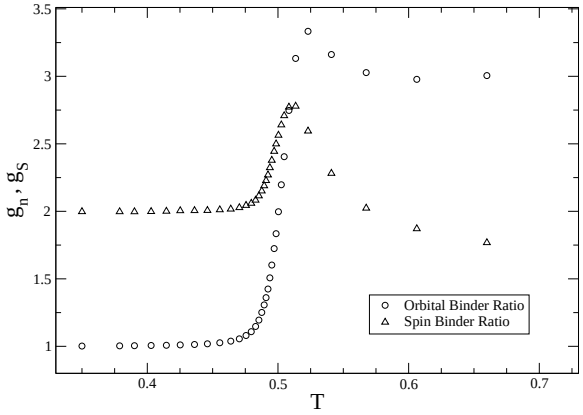

FIG. 12: For an anisotropic ($\lambda = 0.75$) 24×24 system, we plot the orbital and spin binder ratios, g_n and g_S. g_n and g_S both develop what seem like a divergence at the transition temperature. The development of such an incipient divergence is an indicator of a first order transition.

Next we discuss the determination of the order of the transition that motivates our phase diagram for the pnictides. At a second order phase transition, various thermodynamic quantities develop power law singularities characterized by critical exponents, in this case ν and γ. We arrive at Fig. 4 by varying critical exponents until a collapse of all points is achieved. In the case of anisotropy, there are no critical exponents that produce a good data collapse, an indication that the transition is not second order. To support the claim that the anisotropy leads to first order transitions, we show a plot of binder ratios for spin-space anisotropy ($\lambda = 0.75$) in Fig.12. The binder ratio for spins develops a divergence near T_c that is accompanied by a weak divergence for the orbital binder ratio. On its own, this method does not conclusively establish the first order nature of the transition. However, in conjunction with the lack of critical exponents, we propose the phase diagram in Fig. 10. Larger system sizes would be helpful in further studying the divergence of binder ratios in Fig.9 and Fig 12.[97]